Spiral magnetic structure in the iron diarsenate $LiFeAs_2O_7$: A neutron diffraction study

Gwenaëlle Rousse,[1,2,3,*] Juan Rodríguez-Carvajal,[4] Calin Wurm,[5] and Christian Masquelier[3,5]

[1]*Institut de Minéralogie et de Physique des Milieux Condensés (IMPMC), UMR 7590 CNRS-Université Pierre et Marie Curie UPMC Univ Paris 06, Case courrier 115, 4 Place Jussieu, 75252 Paris Cedex 05, France*

[2]*Collège de France, 11 place Marcelin Berthelot, 75231 Paris Cedex 05, France*

[3]*Réseau sur le Stockage Electrochimique de l'Energie (RS2E), FR CNRS 3459, France*

[4]*Institut Laue-Langevin (ILL), Diffraction Group, 6, rue Jules Horowitz, BP 156, 38042 Grenoble Cedex 9, France*

[5]*Laboratoire de Réactivité et Chimie des Solides, CNRS UMR 6007, Université de Picardie Jules Verne, 33 rue Saint-Leu, 80039 Amiens, France*

(Received 9 October 2013; revised manuscript received 26 November 2013; published 31 December 2013)

The magnetic structure of $LiFeAs_2O_7$ (monoclinic, space group $C2$) has been solved using neutron powder diffraction. This compound presents an antiferromagnetic behavior characterized by a long-range ordering observed in the neutron diffraction patterns below the Néel temperature ($T_N = 35$ K). The magnetic structure is found to be incommensurate with respect to the nuclear structure, the magnetic peaks being indexed with a propagation vector $\mathbf{k} = (0.709, 0, 0.155)$. The magnetic moments form a general spiral (helical-cycloidal) arrangement with a constant magnetic moment of 4.21 μ_B. The magnetic structure is discussed in terms of super-super exchange interactions involving two oxygen atoms belonging to an AsO_4 tetrahedron, and compared with the magnetic structure of the di-phosphate analogue $LiFeP_2O_7$. The presence of triangular super-super exchange paths is believed to be at the origin of this incommensurate magnetic structure. The potential of $LiFeAs_2O_7$ as a possible multiferroic material is discussed.

DOI: 10.1103/PhysRevB.88.214433 PACS number(s): 61.05.fm, 75.25.−j

I. INTRODUCTION

The magnetic ordering state is the result of a complex system of quantum mechanical interactions: exchange interactions and anisotropy terms due to relativistic spin-orbit coupling. The prediction of the ground state, given the crystal structure, is not an easy task as it needs full electronic structure calculations; however, simpler mean-field calculations may help to get some insight into the relative strengths of the interactions. The seminal works of Yoshimori, Villain, Lyons, Kaplan, and Freiser[1–4] in the early 1960s on the general problem of determining the classical magnetic ground state of materials (applicable for high spin values), in which super and super-super exchange magnetic interactions are known, have paved the way to understand the magnetic structures of phosphates, silicates, sulfates, arsenates, borates, or more generally oxides.[5–10] If most compounds present rather simple magnetic structures, some are more exotic, displaying incommensurate propagation vectors. In recent years, much attention has been paid to compounds presenting a small magnetic moment ($S = 1/2$, maximum quantum effects) and geometric frustration such as pyrochlore and Kagomé arrangements which may present spin glass behavior, spin quantum liquid ground state, or various long-range magnetic order configurations.[11] On the other hand, the coupling of magnetic and electric properties, giving rise to multiferroic behavior, has promoted a huge interest in the solid state community.[12]

We present here the occurrence of an incommensurate magnetic structure in a relatively simple compound: the iron diarsenate $LiFeAs_2O_7$. This compound was originally studied because it may undergo reversible electrochemical Li^+ insertion associated with the Fe^{3+}/Fe^{2+} redox couple, when used as a cathode material for Li-ion batteries.[13] Our interest here is related to the fact that it presents super-super-exchange (more than one anion in the exchange path) interactions between iron atoms involving diarsenate groups (made of two corner-sharing AsO_4 tetrahedra) that are, in principle, weaker than super-exchange interactions. Moreover, the compound is non-centrosymmetric so that its behavior under an applied field may be interesting from the point of view of multiferroic properties. Understanding its magnetic structure, which appears to be unusually complex with respect to its analogue $LiFeP_2O_7$, will definitely improve the knowledge on this compound.

II. EXPERIMENT

Sample preparation. $LiFeAs_2O_7$ was prepared through a "wet" method based on mixing stoichiometric aqueous solutions of precursors followed by thermal treatments, which generally leads to pure compounds at a lower temperature than that required for solid-state reactions, resulting in the formation of smaller particles with higher surface area. The precursors used were $Li(CH_3COO)$, $NH_4H_2AsO_4$, and $Fe(NO_3)_3.9H_2O$, dissolved in demineralized water. Pure submicronic powders of $LiFeAs_2O_7$ could be obtained at temperatures as low as 300 °C and further annealed at 600 °C to yield particles with higher crystallinity.

Neutron diffraction. Neutron diffraction experiments were performed on $LiFeAs_2O_7$ at the Institute Laue-Langevin (ILL, Grenoble, France), on the high-resolution powder diffractometer D1A (with a wavelength of 1.91 Å) for the study of the nuclear structure at room temperature (far above T_N). The study of the magnetic structure as a function of temperature was undertaken on the high-flux powder diffractometer D1B (ILL). A standard orange cryostat was used to vary the temperature between 2 and 300 K, and a wavelength of 2.52 Å was obtained by using a highly oriented pyrolytic graphite monochromator. For both D1A and D1B experiments, the powdered sample was placed inside a vanadium can of 8 mm of diameter. The program FULLPROF[14] was used for crystal and magnetic structure refinements using the Rietveld method.[15]

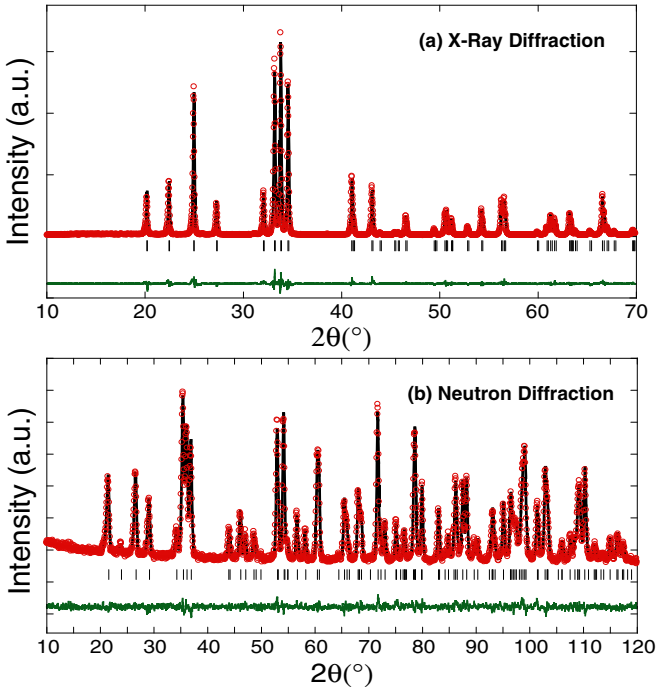

FIG. 1. (Color online) Rietveld refinement of $LiFeAs_2O_7$ (a) against an x-ray diffraction pattern, recorded on a Bruker D8 diffractometer (Co $K\alpha$ radiation, $\lambda_1 = 1.7892$ Å, $\lambda_2 = 1.7932$ Å); (b) against neutron powder diffraction data recorded at 300 K (high-resolution D1A diffractometer, $\lambda = 1.9104$ Å). Calculated (continuous black line) and experimental (red circles) intensities are plotted. Black tick marks correspond to Bragg positions of space group $C2$.

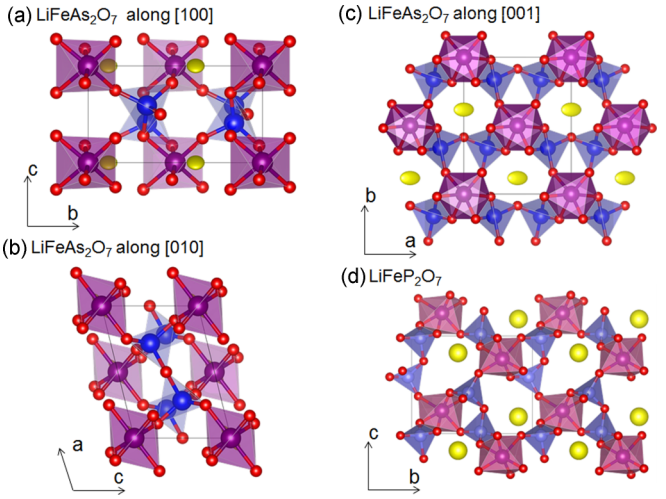

FIG. 2. (Color online) Crystal structure of $LiFeAs_2O_7$ viewed along the (a) [100] direction, (b) [010] direction, and (c) [001] direction (contrary to what one may think when looking in this direction, there is no edge sharing between AsO_4 and FeO_6). Lithium ions (yellow ellipsoids) are located in tunnels delimited by FeO_6 octahedra (in purple) and AsO_4 tetrahedra (in blue) linked by vertices to form diarsenate As_2O_7 groups, as can be seen from (c). (d) Structure of the phosphate analog $LiFeP_2O_7$. PO_4 tetrahedra are shown in blue.

III. RESULTS AND DISCUSSION

A. Nuclear structure of $LiFeAs_2O_7$

The x-ray diffraction pattern of $LiFeAs_2O_7$ indicates that the powder was pure and well crystallized. The powder pattern was fully refined starting from the structural model obtained from single crystal diffraction,[16] in the polar space group $C2$ [Fig. 1(a)]. A concomitant refinement of the structure from high-resolution neutron diffraction data (D1A) was performed leading to the same structural model [Fig. 2], but in addition allowed a precise determination of the lithium positions in the cell [Fig. 1(b)]. The absence of a center of symmetry in the structure was verified by the authors of Ref. 16 using second harmonic generation experiments. We further checked this with a pseudo-symmetry search using the Bilbao Crystallographic Server (program PSEUDO)[17] and confirmed that the crystal structure is polar, hence having the possibility of presenting a spontaneous electric polarization. In order to determine which atoms break the inversion center, the enantiomorph of the original structure was simulated by adding an inversion center at the origin of the cell, even though the two enantiomorphs give rise to the same powder pattern. By comparing these two structures, it appears that three atoms are at the origin of the polarity: Li, As, and one of the four crystallographically distinct oxygen atoms (O4), which bridges the diarsenate group. The rest of the atoms, i.e., the FeO_6 octahedra, form a structure which is centrosymmetric. When trying to force the structure to be symmetrical (space group $C2/c$) with the PSEUDO program, the resulting hypothetical structure breaks the AsO_4 tetrahedral groups and it does not fit the powder pattern at all.

The resulting structural parameters and atomic positions deduced from the high-resolution neutron powder diffraction refinement are reported in Table I. The single crystallographic Fe site is located at the middle of the O_6 octahedron, with Fe-O distances ranging from 1.94(1) to 2.04(1) Å, typical of iron in the Fe^{3+} valence state in octahedral coordination. This is confirmed by a bond valence sum analysis[18] (Table I). Each FeO_6 octahedron is connected to six diarsenate As_2O_7 groups, so that only super-super-exchange type interactions will occur between Fe atoms in this structure. Lithium ions adopt a tetrahedral coordination, they sit in large tunnels running along [001], and display highly anisotropic thermal parameters as depicted by the elongated ellipsoid along the [100] direction [Figs. 2(a)–2(c)]. This reflects the interest of this compound as a Li-ion positive electrode material, as Li ions can easily move within the framework.

It is interesting to compare the structure adopted by the title compound to that of the phosphate analogue, $LiFeP_2O_7$ [Fig. 2(d)] which also crystallizes in a non-centrosymmetric space group, $P2_1$. Lithium ions are located inside the tunnels defined by diphosphate groups P_2O_7. The main difference between the phosphate and the arsenate analogues is that, for the phosphate, one of the P_2O_7 groups is bidentate (i.e., it connects two oxygen atoms belonging to the same FeO_6 octahedron), so that the cavities are more elongated than in the arsenate, for which FeO_6 octahedra are linked to six different As_2O_7 groups. Therefore replacing P with As leads to a distinct framework, which may be due to the larger AsO_4 groups as compared to the PO_4 groups (As−O 1.68 Å vs P−O 1.53 Å) and/or to the occupation of the $3d^{10}$ configuration for As^{5+}.

TABLE I. Crystallographic data and atomic positions of $LiFeAs_2O_7$ resulting from refinements of the structure against the data collected on the high-resolution neutron powder diffractometer D1A (ILL, Grenoble, France) obtained at room temperature with a wavelength of $\lambda = 1.9104$ Å ($R_{Bragg} = 2.39\%$, $\chi^2 = 1.09$). Results from the bond valence sum analysis (BVS) are also indicated.

Space group						*C*2
a (Å)						6.6786(1)
b (Å)						8.2855(1)
c (Å)						4.7429(1)
α (deg)						90
β (deg)						103.950(1)
γ (deg)						90
V (Å^3)						254.708(5)
Atom	Wyckoff	*x*	*Y*	*z*	B_{iso} (Å^2)	BVS
Li	*2a*	0	0.617(2)	0	*[a]	0.78(2)
Fe	*2a*	0	0	0	0.21(5)	3.14(2)
As	*4c*	0.7824(3)	0.3370(5)	0.5910(5)	0.35(5)	5.04(3)
O1	*4c*	0.7497(3)	0.4811(5)	0.8237(5)	0.40(6)	1.97(2)
O2	*4c*	0.8310(4)	0.1567(5)	0.7473(6)	1.14(6)	1.94(2)
O3	*4c*	0.6100(4)	0.3170(5)	0.2773(6)	0.25(6)	2.00(2)
O4	*2b*	0	0.4147(6)	½	1.06(9)	2.17(2)

[a]Anisotropic β ($\times 10^4$): $\beta_{11} = 275(58)$, $\beta_{22} = 84(29)$, $\beta_{33} = 178(86)$, $\beta_{12} = 0$, $\beta_{13} = -132(55)$, $\beta_{23} = 0$.

B. Magnetic measurements

The temperature dependence of the magnetic susceptibility for the title compound is shown in Fig. 3(a). In a field of 500 G, it shows cusps indicative of the onset of antiferromagnetic ordering at about 35 K. Below 5 K, $LiFeAs_2O_7$ shows sharp upturns characteristic of a paramagnetic contribution which is likely generated by imperfections in the crystal and/or a magnetic structure that may contain non-ordered Fe^{3+} ions. It should also be noted that the zero-field cooled (zfc) and field-cooled (fc) traces perfectly overlap.

The high-temperature region (150 to 350 K) of the inverse susceptibility, obtained in a field of 500 G, was fit to the Curie-Weiss equation, $\chi = C/(T - \Theta_{CW})$, in order to examine the spin state of iron and the relative strengths of the interactions [Fig. 3(b)]. An effective moment of 6.0(1) μ_B per Fe is found. This value can be compared with the spin-only effective moment of 5.92 μ_B expected for a single high-spin Fe^{3+} in an octahedral coordination environment (d^5, $t_{2g}^3 e_g^2$, $S = 5/2$, $L = 0$). A Curie-Weiss Θ_{CW} of $-77(1)$ K is obtained for $LiFeAs_2O_7$, reflecting strong antiferromagnetic correlations between iron atoms. The value of the ratio $|\Theta_{CW}/T_N| \approx 2.2$ indicates a small degree of frustration in the magnetic structure. The good fit with the Curie Weiss law down to nearly T_N indicates that negligible short-range order builds up due to frustration above T_N.

C. Magnetic structure of $LiFeAs_2O_7$

In order to solve the magnetic structure of the title compound, high-intensity neutron diffraction measurements were performed on the diffractometer D1B at ILL, which is especially devoted to this kind of study as it presents a good resolution at low angles. The patterns collected below T_N on $LiFeAs_2O_7$ show the appearance of many extra reflections at low angles (Fig. 4). Unlike the phosphate analogue, these reflections cannot be indexed with a high symmetry propagation vector at special points of the Brillouin zone which would correspond to a magnetic cell commensurate with the nuclear one. We used the program K-SEARCH (distributed within the FULLPROF suite[14]) to determine the propagation vector **k**. We found that the only propagation vector which could index all the magnetic peaks was $\mathbf{k} = (X, Y, Z) = (0.709, 0, 0.155)$, so that the magnetic structure is incommensurate with respect to the nuclear one. The propagation vector lies

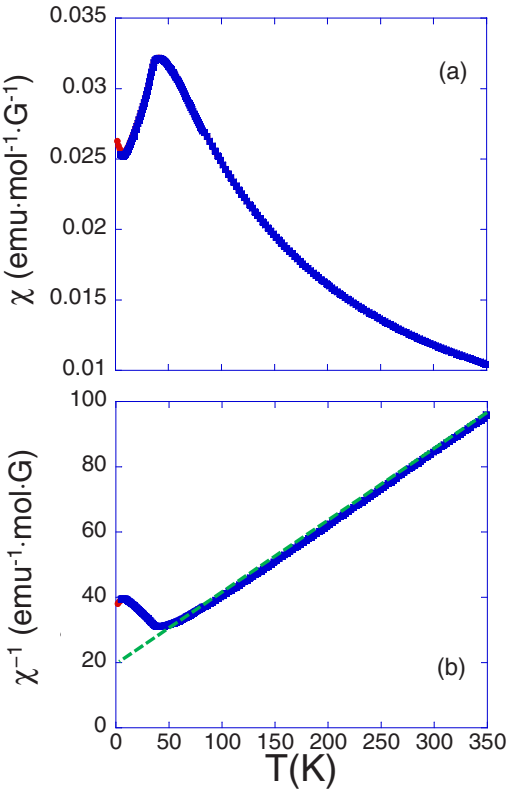

FIG. 3. (Color online) (a) Susceptibility curves of $LiFeAs_2O_7$ as a function of temperature, under a magnetic field of 500 G. Blue and red symbols are zero field cooled and field cooled, respectively. (b) Inverse of susceptibility as a function of temperature, between 2 and 350 K, under a magnetic field of 500 G. The green dotted line is the Curie Weiss fit of the high-temperature region (150–350 K).

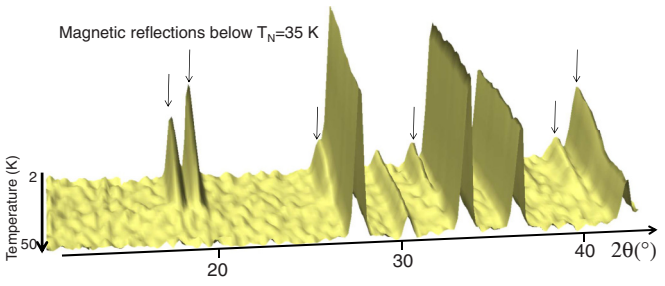

FIG. 4. (Color online) Neutron diffraction patterns of $LiFeAs_2O_7$ (D1B, $\lambda = 2.52$ Å) between 2 and 50 K, showing the appearance of magnetic peaks (highlighted with arrows) below the Neel temperature of 35 K.

in the (**a***, **c***) plane. We can notice that $X + 2Z$ is close to 1, but if we impose this constraint ($X + 2Z = 1$) in the refinement, the magnetic peaks are clearly shifted from their experimental 2θ position. Therefore the propagation vector shows no specificity except that its Y component is zero.

A symmetry analysis[19] does not provide restrictions to the orientation of the magnetic moments of the Fe^{3+} ions. Indeed there is only a single small representation of dimension 1 and a single Bravais lattice (only one atom per primitive cell), thus giving rise to a general complex Fourier coefficient $\mathbf{S_k} = (u, v, w)$ with complex values u, v, w. If the real and imaginary components of $\mathbf{S_k}$ are parallel we obtain sinusoidal structures, and if they are perpendicular we obtain spiral structures.

We tried different models for the magnetic structure. It appears that the solutions with sinusoidal structures gave magnetic moments abnormally high for Fe^{3+}, and hence were not further considered. After several trials concerning the spiral structures, we found that the spiral axis (to which the magnetic moments are perpendicular) is not along a specific simple direction of the crystal. Moreover, this axis is not along the propagation vector, so that the spiral magnetic structure is neither a pure helix nor a pure cycloid. We used simulated annealing techniques to determine the possible axes of the spiral: it led to four possibilities that could account for the observed magnetic reflections which correspond to only two spiral orientations, as shown later. Let us consider an orthonormal Cartesian system ($\mathbf{a}_O$, $\mathbf{b}_O$, $\mathbf{c}_O$) attached to the monoclinic crystallographic cell (**a**, **b**, **c**), so that we can define spherical (θ, φ) angles. In our convention, $\mathbf{a}_O$ (respectively $\mathbf{b}_O$) is parallel to **a** (respectively **b**) and $\mathbf{c}_O$ is defined by $\mathbf{a}_O \times \mathbf{b}_O$. The four different sets of values for the spherical angles (θ, φ) angles defining the possible spiral axes are the following: ($\theta_1 = 80.0(5)°$, $\varphi_1 = 157.0(5)°$), ($\theta_2 = 100.0(5)°$, $\varphi_2 = 337.0(5)°$), ($\theta_3 = 100.0(5)$, $\varphi_3 = 23.0(5)°$), and ($\theta_4 = 80.0(5)°$, $\varphi_4 = 203.0(5)°$). Looking carefully at these different possibilities, it appeared that the second, third, and fourth can easily be deduced from the first as ($\theta = 80.0(5)°$, $\varphi = 157.0(5)°$), ($\pi - \theta$, $\pi + \varphi$), ($\pi - \theta$, $\pi - \varphi$), and (θ, $2\pi - \varphi$). One can further notice that only two orientations have to be considered, as the two others give the same spiral axis, but taken in the opposite direction; it means that they are of opposite chirality (see Fig. 5): magnetic moments on iron atoms turn in the opposite way (left or right) under the effect of the propagation vector when several units cells along **a** or **c** are considered. The two remaining solutions ($\theta_1 = 80.0(5)°$, $\varphi_1 = 157.0(5)°$), and (θ, $2\pi - \varphi$) = ($80.0(5)°$, $203.0(5)°$) correspond to two different spiral directions which are related by the twofold rotation axis which is along [010] in space group $C2$. These two possibilities (together with their different chiralities) lead exactly to the same refinement although they are physically different, but one cannot distinguish them from neutron powder diffraction. In all cases, the magnetic moments are confined to the plane perpendicular to the spiral axis. The refined amplitude value is 4.28(3) μ_B, in good agreement with what is expected for high spin Fe^{3+} ions ($S = 5/2$). The Rietveld refinement from the data recorded at 2 K using the spiral axis ($\theta_1 = 80.0(5)°$, $\varphi_1 = 157.0(5)°$) and a moment of 4.28(3) μ_B perpendicular to the axis is presented in Fig. 6, together with a pattern recorded at 60 K (above T_N) to appreciate the magnetic contribution. The two possible magnetic structures corresponding to the two spiral directions are displayed in Fig. 7. The magnetic moment of the Fe atom at the unit cells with origins given by the vector positions $\mathbf{R}_l = (l_1 + \frac{1}{2}s)\mathbf{a} + (l_2 + \frac{1}{2}s)\mathbf{b} + l_3\mathbf{c}$ (with l_i integers and $s = 0$ or $s = 1$ because we are dealing with a C cell) is calculated in terms of the Fourier coefficient $\mathbf{S_k} = \frac{1}{2}(\mathbf{U} + i\mathbf{V})$ by the expression

$$\mathbf{m}_l = \sum_{\mathbf{k}} \mathbf{S_k} \exp(-2\pi i \mathbf{k}\mathbf{R}_l) = \mathbf{U}\cos(2\pi \mathbf{k}\mathbf{R}_l) + \mathbf{V}\sin(2\pi \mathbf{k}\mathbf{R}_l),$$

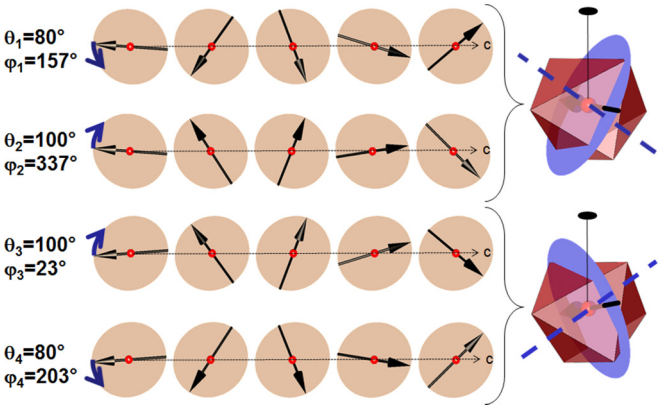

FIG. 5. (Color online) View of the four possible helix-cycloid magnetic structures along the c axis [each with different spherical angles (θ, φ) whose values are written for clarity; see text]. The magnetic moments on iron atoms are displayed as black arrows. Five unit cells are displayed along the c axis to see the effect of the Z component of **k** on the orientation of the magnetic moment. The first two solutions (θ_1, φ_1) and (θ_2, φ_2) correspond to the two different chiralities of the same spiral direction, whereas the two others (θ_3, φ_3) and (θ_4, φ_4) correspond to a spiral axis with is deduced from the first one by the twofold symmetry axis parallel to the [010] direction, as seen in Fig. 7. Note that we cannot distinguish these four solutions from neutron powder diffraction.

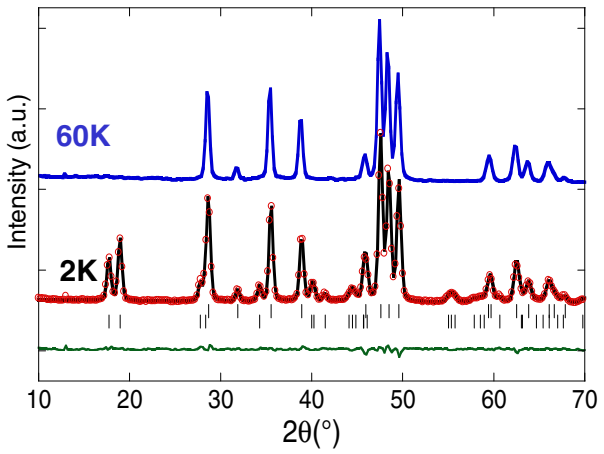

FIG. 6. (Color online) Observed (red circles) versus calculated (black continuous line) neutron powder diffraction patterns of $LiFeAs_2O_7$ (D1B, $\lambda = 2.52$ Å) recorded at 2 K. The positions of the Bragg reflections are represented by vertical bars (first line = nuclear, second line = magnetic). The difference (obs−calc) pattern is displayed in green. The pattern recorded at 60 K (i.e., above the magnetic transition) is displayed for comparison.

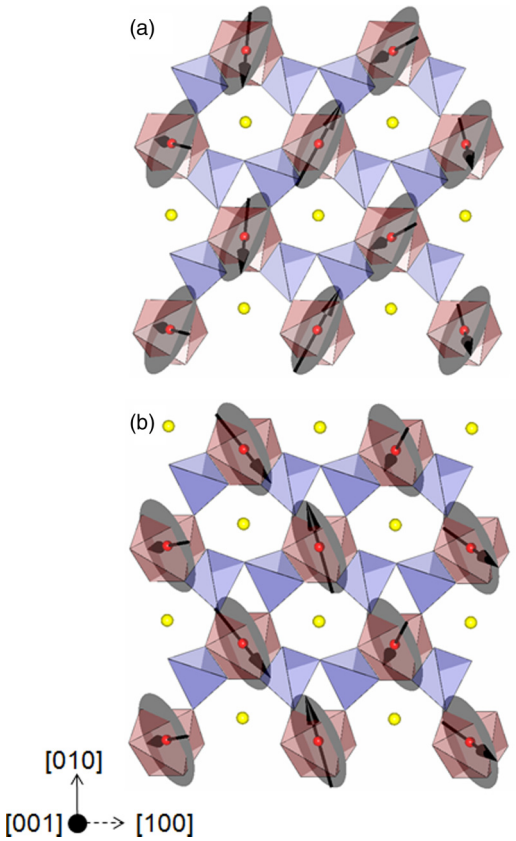

FIG. 7. (Color online) Representation of the two possible spiral (helix-cyloid) magnetic structures for $LiFeAs_2O_7$, viewed along the [001] direction. The spherical (θ, φ) angles defining the spiral direction are (80°, 157°) and (80°, 203°) for (a) and (b), respectively. We can notice that they are symmetric by the twofold symmetry axis parallel to the [010] direction. Arrows indicate the magnetic moments on the iron atoms.

with $\mathbf{U} = (-1.733\,63,\ 0.290\,40,\ -4.343\,67)$ and $\mathbf{V} = (-1.672\,33,\ -3.939\,76,\ 0.0)$ for the (80°, 157°) case and $\mathbf{U} = (-1.733\,63,\ -0.290\,40,\ -4.343\,67)$ and $\mathbf{V} = (1.672\,33,\ -3.939\,76,\ 0.0)$ for the (80°, 203°) case. The vectors **U** and **V** are given with components in Bohr magnetons (μ_B) with respect to the unitary basis with axes along the conventional cell: (**a**/a, **b**/b, **c**/c). Therefore, in both magnetic structures, the absolute values of the magnetic moments are the same for all iron atoms, only the orientation of the moments changes from one atom to another when the structure is seen perpendicular to the [010] direction (Fig. 8), as a result of the $\mathbf{k} = (X,0,Z)$ propagation vector. Note that none of the two spiral axes [$\theta = 80.0(5)°$, $\varphi = 157.0(5)°$, and $\varphi = 203.0(5)°$] have a simple expression in terms of [hkl] directions. The angle between the spiral axis and the propagation vector is $\omega = 46.5°$, so that the magnetic structure is intermediate between a pure helical ($\omega = 0.0°$) and pure cycloidal structure ($\omega = 90.0°$).

In the phosphate analogue $LiFeP_2O_7$, the magnetic structure was found to be rather simple with a magnetic propagation vector $\mathbf{k} = (0,0,0)$ and an almost collinear arrangement of the magnetic moments along the [100] direction of the $P2_1$ cell.[20] We address now the question of why the diarsenate compound is so different in terms of magnetic arrangement.

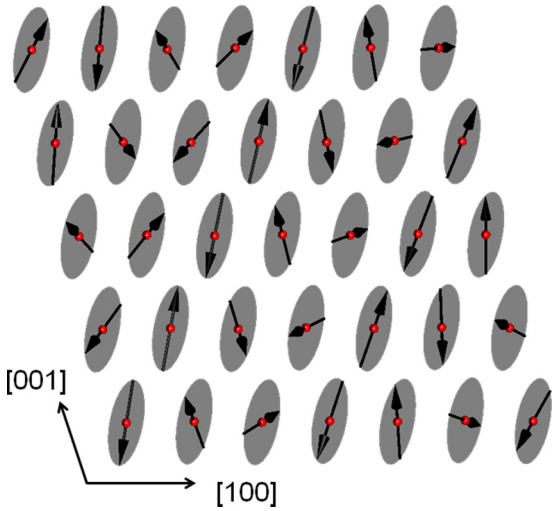

FIG. 8. (Color online) Representation of the magnetic structure for $LiFeAs_2O_7$ with spherical angles (θ, φ) = (80°, 157°). This representation clearly shows the change in the moment's orientation due to the propagation vector $\mathbf{k} = (0.709, 0, 0.155)$.

D. Analysis and discussion of the magnetic structure

In order to understand the origin of the incommensurate magnetic structure, we decided to examine the exchange paths between iron atoms in $LiFeAs_2O_7$. A C centered Bravais lattice and iron positioned at the origin of the cell lead to three different isotropic super-super-exchange interactions (J_i, $i = 1,2,3$), numbered in ascending order of distances between magnetic atoms. The exchange paths differ by changes in distances or in (Fe-O_i-O_j), (O_iO_j-Fe) angles and (Fe-O_i-O_j-Fe) torsion angles (Table II). The shortest isotropic exchange interaction, J_1, connects the two iron atoms which are related with the (0, 0, 1) lattice translation, via O1 and O3. J_2 connects iron atoms that belong to the same "ring" in the (**a**, **b**) plane via O1 and O2; J_3 is the largest distance that had to be considered: it connects two iron atoms related by the lattice translation (½, ½, 1) via O2 and O3, of special importance for the helix-cycloid magnetic structure. A scheme of the interactions J_1, J_2, and J_3 is shown in Fig. 9. The topology (how iron atoms are connected through these three different exchange paths) is similar to the one encountered in the phosphate analogue $LiFeP_2O_7$, which is represented in Fig. 10. There are, however, a few differences: for the phosphate analogue, only the exchange integrals J_1 and J_2 had to be taken into account to get the $\mathbf{k} = (0, 0, 0)$ observed magnetic structure as ground state. The exchange integral J_3 should be very weak in the phosphate because no simple super-super-exchange paths exist through the phosphate groups. Note that a topology with only J_1 and J_2 can generate only commensurate structures, as is the case for $LiFeP_2O_7$, because these two exchange integrals create a non-frustrated 3D network. The introduction of J_3 creates an additional path that generates a triangular topology that may be at the origin of some degree of frustration, and therefore leads to the observed helical-cycloidal magnetic structure. Moreover, the geometrical characteristics of the exchange path for J_3 in $LiFeAs_2O_7$ (see Table II) are more favorable (stronger orbital overlap) than for the other two J_1, J_2 paths.

TABLE II. List of effective exchange interactions considered between iron atoms and related super-super-exchange paths, bond lengths (in Å) and angles (expressed in °) in $LiFeAs_2O_7$. The translational part to obtain the position of the second iron atom is indicated.

Interaction	Path	d_1	d_2	d_3	α_1	α_2	γ	d
J_1	Fe-O1-O3-Fe along **c**	2.04	2.87	2.02	106.6	102.7	− 86.4	4.74
J_2	Fe-O2-O1-Fe along $\frac{1}{2}(\mathbf{a}+\mathbf{b})$	2.04	2.78	1.93	109.3	132.1	89.0	5.32
J_3	Fe-O2-O3-Fe along $\frac{1}{2}(\mathbf{a}+\mathbf{b}+2\mathbf{c})$	2.03	2.71	1.93	160.5	163.8	134.6	6.57

$d_1 = d(\text{Fe-O}_i)$, $d_2 = d(\text{O}_i\text{-O}_j)$, $d_3 = d(\text{O}_j\text{-Fe})$, $\alpha_1 = (\text{Fe-O}_i\text{-O}_j)$, $\alpha_2 = (\text{O}_i\text{-O}_j\text{-Fe})$, γ = torsion angle, $d = d(\text{Fe-Fe})$.

The problem of the magnetic ground state of a system of classical spins connected by isotropic exchange interactions was considered 40 years ago by several authors.[2,21] The first ordered state can be obtained from the resolution of an eigenvalue problem where the matrix is the Fourier transform of the exchange interactions. In the case of a simple Bravais lattice, the first ordered magnetic state is also the ground state (this is the so-called Villain-Yoshimori theorem).[1,4] We have used the method discussed in Ref. 22 to evaluate the conditions to be satisfied by the exchange integrals J_i in order to have the propagation vector **k** as the ground state. The full treatment is performed in the Appendix. In our case, $\mathbf{k} = (0.709, 0, 0.155)$ is the observed propagation vector and it must correspond to the state of the lowest energy. This occurs when J_1, J_2, and J_3 are negative, and obey the following conditions which were analytically deduced: $J_2 \approx 0.522\ J_1$ and $J_3 \approx 6.932\ J_1$ [see Appendix, Eq. (A8)]. If the conditions are not fulfilled, then the propagation vector giving the lowest energy will be simpler, e.g., (1, 0, 0). In order to get further insight on why the propagation vector is $\mathbf{k} = (X, Y, Z) = (0.709, 0, 0.155)$ we plotted the energy [obtained from Eq. (A2) in the Appendix, but with $Y = 0$) defined as

$$\xi(\mathbf{k}, J_1, J_2, J_3) = -2J_1 \cos 2\pi Z - 4J_2 \cos \pi X - 4J_3 \cos \pi (X + 2Z)$$

as a function of X and Z, for an arbitrary negative value of J_1 and corresponding values of (J_2, J_3) taken as $J_1 = -1$, $J_2 = -0.522$, and $J_3 = -6.932$ (see Appendix). The **k** vectors were varied in the (X, 0, Z) plane with X in [0, 1] and Z in [0, ½], and Fig. 11 gathers the resulting energy $\xi(\mathbf{k}, J_1, J_2, J_3)$ as a high-dimensional phase diagram using X and Z as Cartesian axes. It appears clearly that the propagation vector **k** is in a region with relative low energy which looks like a valley pointing between the propagation vectors (0, 0, ½) and (1, 0, 0).

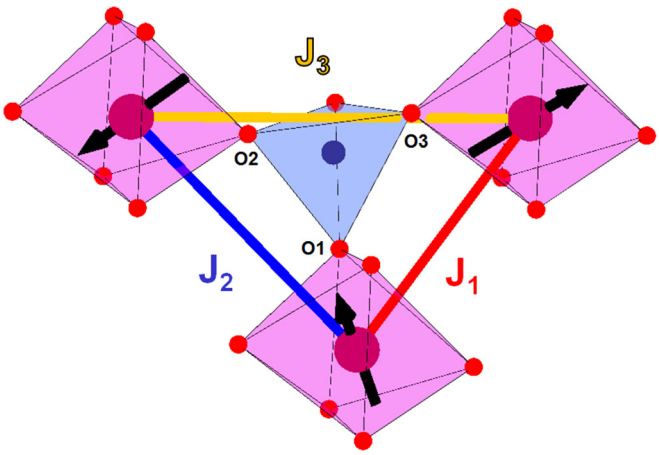

FIG. 9. (Color online) Representation of three exchange paths between iron atoms in $LiFeAs_2O_7$. J_1 (in red) connects two translational equivalent atoms along [001], J_2 (in blue) connects iron atoms belonging to the "rings," and J_3, the longest one, is displayed in yellow. J_3 presents angles much more linear then J_1 and J_2 (see values in Table II).

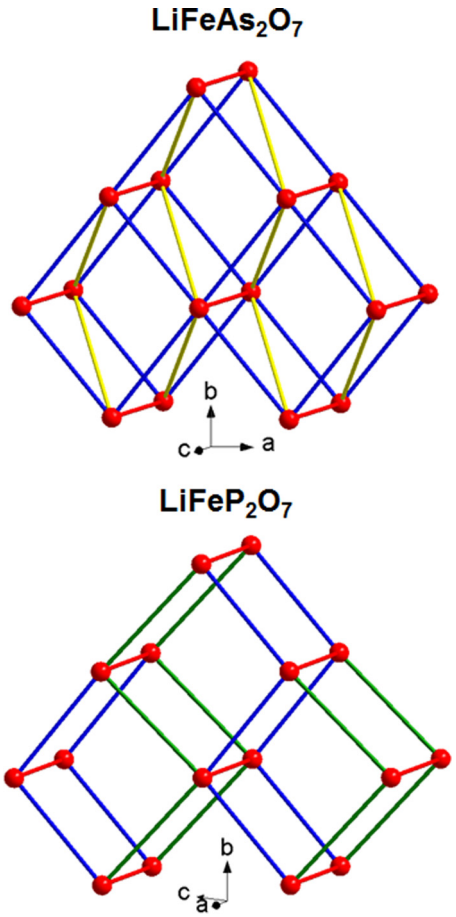

FIG. 10. (Color online) Topology of $LiFeAs_2O_7$ (top) and $LiFeP_2O_7$ (bottom). Iron atoms are displayed as red balls. For the arsenate counterpart, we have indicated J_1 in red (along [001]), J_2 in blue (along [½ ½ 0]), and J_3 in yellow (along [½ ½ 1]). All of them are of super-super-exchange type. For the phosphate analog, three exchange integrals were considered (Ref. 20) that correspond to J_1 (in red), and two others (displayed in blue and green) that are equivalent to J_2 in the arsenate.

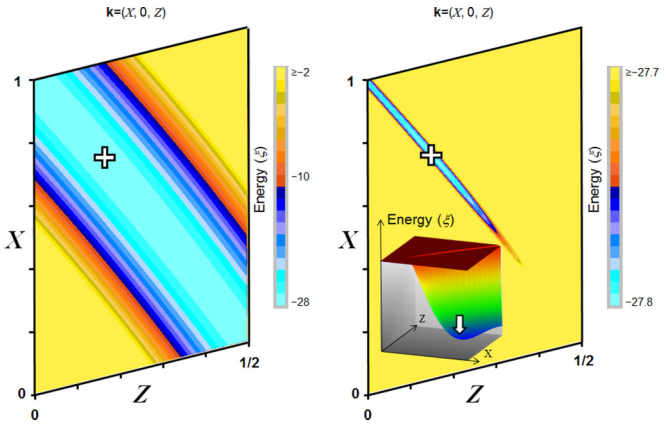

FIG. 11. (Color online) Plot of the energy $\xi(\mathbf{k}, J_1, J_2, J_3)$ as a function of the X and Z components of the propagation vector $\mathbf{k} = (X, 0, Z)$, for exchange integrals values taken as $J_1 = -1$, $J_2 = -0.522$, and $J_3 = -6.932$ (see text and Appendix). The energy is displayed on a color scale in units of J_1. The left panel shows a wide range of energy (between -27.8 and 0), while the right one displays a color scale extremely reduced to focus on the lowest energies (between -27.8 and -27.7). The white crosses show the position of the experimental $\mathbf{k}$ vector: $X = 0.709$ and $Z = 0.155$. The inset in the right panel shows a three-dimensional plot of ξ. The $\mathbf{k}$ vectors were varied in the $(X, 0, Z)$ plane with the white arrow pointing to the experimental $\mathbf{k}$ vector, lying in the deepest region of the valley (global minimum of energy).

A global view of the $\xi(\mathbf{k}, J_1, J_2, J_3)$ surface (Fig. 11, left) does not show clearly the existence of a minimum at the observed position; however, looking at the lowest range of energies we detected the presence of a shallow global minimum centered at $\mathbf{k} = (0.709, 0, 0.155)$. The valley does not follow the equation $X + 2Z = 1$; it is slightly curved when seen from [1 0 ½] (Fig. 11, right).

The form of the valley and the scale of energies indicate that a small external perturbation, such as pressure, would more likely change the magnetic propagation vector into a simpler one, and as a consequence break the spiral magnetic ordering. The orientation of the spiral with respect to the lattice and the propagation vector (halfway between an helix and a cycloid) should result from additional Dzyaloshinskii-Moriya interactions, as reported for other systems, such as Cu-based systems,[23–25] molecular magnets,[26] and some metals.[27]

Lastly, we would like to mention that the di-phosphate analogue $LiFeP_2O_7$, despite having a different structure as explained above, is also polar. It displays a simple magnetic structure, and it has been recently shown from a single crystal study that it presents some magnetocaloric effects and interesting functional properties.[28,29] Therefore $LiFeAs_2O_7$ would be a very good candidate for studying also such kind of properties. It is known that the Dzyaloshinskii-Moriya interactions, via the establishment of unconventional long-range magnetic order, also favor the occurrence of multiferroic properties.[30,31] Single crystals of the arsenate could therefore be very valuable, provided that they can be grown and that risks associated with the As^{3+} ions can be carefully mastered. Also they would be necessary in order to discriminate between the different structural and magnetic chiralities using full neutron 3D polarimetry. Moreover, the study of the behavior of the magnetic structure under applied electric and magnetic fields will help to get more insight into the properties of this compound.

IV. CONCLUSION

The lithium-iron diarsenate $LiFeAs_2O_7$ presents a magnetic phase transition at 35 K that we have studied by means of neutron powder diffraction. $LiFeAs_2O_7$, despite having a magnetic topology very similar to the phosphate analogue $LiFeP_2O_7$, presents a completely different magnetic structure, which is incommensurate with a propagation vector $\mathbf{k} = (0.709, 0, 0.155)$. Magnetic moments follow a spiral (helix-cycloid), the axis of which does not point along a specific crystallographic axis. From powder diffraction we get two possible spiral axes deduced by the twofold symmetry axis of the polar space group $C2$. As $LiFeAs_2O_2$ crystallizes in a polar structure, it is a candidate for being a potential multiferroic compound. The analysis of the topology and of the exchange paths in $LiFeAs_2O_7$ indicates that three super-super-exchange interactions have to be considered. The presence of a topology with triangular paths induces frustration effects that are at the origin of the incommensurate magnetic structure.

APPENDIX

The first ordered magnetic state is obtained, as a function of $\mathbf{k}$ (on the surface or at the interior of the Brillouin Zone) and the exchange integrals, as the eigenvector corresponding to the lowest eigenvalue of the negative Fourier transform of exchange integral matrix:

$$\xi_{ij}(\mathbf{k}) = -\sum_m J_{ij}(\mathbf{R}_m) \exp\{2\pi i \mathbf{k}\mathbf{R}_m\}. \qquad \text{(A1)}$$

The indices i,j refer to the magnetic atoms in a primitive cell, and $J_{ij}(\mathbf{R}_m)$ is the isotropic exchange interaction (including the modules of the spins) between the spins of atoms i and j in unit cells separated by the lattice vector $\mathbf{R}_m$. Our convention is that negative J_{ij} means antiparallel coupling (pair interaction energy: $E_{ij} = -J_{ij}\mathbf{S}_i\mathbf{S}_j$). If we consider anisotropic exchange interactions, or single ion anisotropy, we have to consider in general a tensor $J_{ij}^{\alpha\beta}(\mathbf{R}_m)$ in which $\alpha,\beta = x,y,z$; instead of the scalar variables $J_{ij}(\mathbf{R}_m)$.

Let us start with the scalar case that corresponds to a very good first approximation (in general $|J_{\text{isotropic}}| > 10^2 |J_{\text{anisotropic}}|$) to determine the propagation vector. In our case we have only one atom per primitive cell; so that the above matrix is very simple (1×1) and the problem can be solved analytically. The eigenvalue coincides with the matrix and it is given by the expression

$$\xi(\mathbf{k}, J_1, J_2, J_3) = -2J_1 \cos 2\pi Z - 4J_2 \cos \pi X \cos \pi Y - 4J_3 \cos \pi(X + 2Z) \cos \pi Y, \qquad \text{(A2)}$$

where X, Y, and Z are the reduced coordinates of the propagation vector $\mathbf{k}$ in the conventional reciprocal basis.

The conditions to get the possible stable magnetic structures are obtained by putting to zero the derivatives of the eigenvalues with respect to the components of $\mathbf{k}$ and forcing

the Hessian to be definite positive so that it corresponds to a minimum in energy. The first set of three equations is given by the expressions

$$\begin{aligned}\frac{\partial\xi}{\partial X} &= 4\pi\cos\pi Y[J_2\sin\pi X + J_3\sin\pi(X+2Z)] = 0,\\ \frac{\partial\xi}{\partial Y} &= 4\pi\sin\pi Y[J_2\cos\pi X + J_3\cos\pi(X+2Z)] = 0,\\ \frac{\partial\xi}{\partial Z} &= 4\pi[J_1\sin 2\pi Z + 2J_3\sin\pi(X+2Z)\cos\pi Y] = 0.\end{aligned} \tag{A3}$$

Irrespective of the values of exchange interactions, the first equation is satisfied with Ycomponent of $\mathbf{k}$ equal to $1/2$ and the second equation is satisfied with $Y = 0, 1$. In order to simplify the discussion we take from the beginning the value $Y = 0$, which is the observed value, so we have two equations from the above set that have to be satisfied by the exchange integrals and the propagation vector components,

$$\begin{aligned}J_2\sin\pi X + J_3\sin\pi(X+2Z) = 0,\\ J_1\sin 2\pi Z + 2J_3\sin\pi(X+2Z) = 0.\end{aligned} \tag{A4}$$

The Hessian matrix (restricted to $Y = 0$ and neglecting a constant factor) can be written as

$$H = \begin{pmatrix} J_2\cos\pi X + J_3\cos\pi(X+2Z) & 0 & 2J_3\cos\pi(X+2Z) \\ 0 & J_2\cos\pi X + J_3\cos\pi(X+2Z) & 0 \\ 2J_3\cos\pi(X+2Z) & 0 & 2J_1\cos 2\pi Z + 4J_3\cos\pi(X+2Z) \end{pmatrix}. \tag{A5}$$

For the stability of the magnetic structure all the eigenvalues of the Hessian matrix should be positive. The eigenvalues are obtained by solving the equation $\det(H-\lambda I) = 0$. This equation can be written as

$$\begin{aligned}\det(H-\lambda I) &= \begin{vmatrix} \alpha-\lambda & 0 & \beta \\ 0 & \alpha-\lambda & 0 \\ \beta & 0 & \gamma-\lambda \end{vmatrix}\\ &= (\alpha-\lambda)(\lambda^2-(\alpha+\gamma)\lambda+\alpha\gamma-\beta^2) = 0.\end{aligned} \tag{A6}$$

in which the coefficients α, β, and γ are shorthand notations for the terms appearing in the Hessian. The eigenvalues (all of them should be positive) are

$$\begin{aligned}&\lambda_1 = \alpha > 0, \quad 2\lambda_2 = \alpha+\gamma+\sqrt{(\alpha-\gamma)^2+4\beta^2} > 0,\\ &2\lambda_3 = \alpha+\gamma-\sqrt{(\alpha-\gamma)^2+4\beta^2} > 0.\end{aligned} \tag{A7}$$

In our case the propagation vector is $\mathbf{k} = (0.709, 0, 0.155)$; assuming that Eqs. (A4) and (A7) are satisfied by the components $X_o = 0.709$ and $Z_o = 0.155$, we obtain the following conditions for the exchange integrals:

$$\begin{aligned}J_2 &= \frac{\sin 2\pi Z_o}{2\sin\pi X_o}J_1 = a_{21}J_1 \approx 0.522J_1,\\ J_3 &= -\frac{\sin 2\pi Z_o}{2\sin\pi(X_o+2Z_o)}J_1\\ &= -a_{31}J_1 \approx -(-6.932)J_1 \approx 6.932J_1.\end{aligned} \tag{A8}$$

From the first equation of (A7),

$$\begin{aligned}&J_2\cos\pi X_o + J_3\cos\pi(X_o+2Z_o)\\ &\quad = -0.6104J_2 - 0.9982J_3 > 0.\end{aligned} \tag{A9}$$

From (A8) we see that all exchange integrals have the same sign, and from (A9) we obtain that all of them are negative (antiferromagnetic interactions) and, as a consequence, the origin of the incommensurability appears to be the frustrated topology that forms triangular paths as shown in Fig. 10.

The stability condition for the observed $\mathbf{k}$ is granted for negative J_i's satisfying Eqs. (A8), as one can verify by substituting the values in the remaining equations of (A7). The values of α, β, and γ for $\mathbf{k} = (X_o, 0, Z_o)$ satisfying (A8) can be written as

$$\begin{aligned}\alpha &= -0.6104J_2 - 0.9982J_3 = a_2 + a_3,\\ \beta &= -1.996\,44J_3 = 2a_3,\\ \gamma &= 2J_1\cos 2\pi Z_o + 4J_3\cos\pi(X_o+2Z_o)\\ &= -0.5095J_1 - 3.992\,88J_3 = a_1 + 4a_3.\end{aligned} \tag{A10}$$

For λ_2 we have a positive value because the square-root term is positive, and both $\alpha, \gamma > 0$. For λ_3, after some algebra, we have the equivalent following condition:

$$a_1a_2 + a_1a_3 + 4a_2a_3 > 0.$$

One can see that this is verified because all a_i are positive for negative J_i's [see Eq. (A10)].

*Author to whom correspondence should be addressed: gwenaelle.rousse@upmc.fr

[1]J. Villain, J. Phys. Chem. Solids **11**, 303 (1959).
[2]D. H. Lyons and T. A. Kaplan, Phys. Rev. **120**, 1580 (1960).
[3]M. J. Freiser, Phys. Rev. **123**, 2003 (1961).
[4]A. Yoshimori, J. Phys. Soc. Jpn. **14**, 807 (1959).
[5]B. C. Melot, G. Rousse, J. N. Chotard, M. Ati, J. Rodriguez-Carvajal, M. C. Kemei, and J. M. Tarascon, Chem. Mater. **23**, 2922 (2011).
[6]B. C. Melot, G. Rousse, J.-N. Chotard, M. C. Kemei, J. Rodriguez-Carvajal, and J.-M. Tarascon, Phys. Rev. B **85**, 094415 (2012).

[7]M. Reynaud, G. Rousse, J. N. Chotard, J. Rodriguez-Carvajal, and J. M. Tarascon, Inorg. Chem. **52**, 10456 (2013).
[8]P. Barpanda, G. Rousse, T. Ye, C. D. Ling, Z. Mohamed, Y. Klein, and A. Yamada, Inorg. Chem. **52**, 3334 (2013).
[9]G. Rousse, J. Rodriguez-Carvajal, C. Wurm, and C. Masquelier, Chem. Mater. **13**, 4527 (2001).
[10]L. Tao, J. R. Neilson, B. C. Melot, T. M. McQueen, C. Masquelier, and G. Rousse, Inorg. Chem. **52**, 11966 (2013).
[11]J. E. Greedan, J. Mater. Chem. **11**, 37 (2001).
[12]S. W. Cheong and M. Mostovoy, Nat. Mater. **6**, 13 (2007).
[13]C. Wurm, M. Morcrette, G. Rousse, L. Dupont, and C. Masquelier, Chem. Mater. **14**, 2701 (2002).
[14]J. Rodriguez-Carvajal, Physica B **192**, 55 (1993).
[15]H. M. Rietveld, J. Appl. Crystallogr. **2**, 65 (1969).
[16]S. L. Wang, C. H. Wu, and S. N. Liu, J. Solid State Chem. **113**, 37 (1994).
[17]C. Capillas, E. S. Tasci, G. de la Flor, D. Orobengoa, J. M. Perez-Mato, and M. I. Aroyo, Z. Kristall. **226**, 186 (2011).
[18]I. D. Brown and D. Altermatt, Acta Crystallogr. Sect. B **41**, 244 (1985).
[19]E. F. Bertaut, Acta Crystallogr. Sect. A **24**, 217 (1968).
[20]G. Rousse, J. Rodriguez-Carvajal, C. Wurm, and C. Masquelier, Solid State Sci. **4**, 973 (2002).
[21]J. Kanamori, J. Phys. Chem. Solids **10**, 87 (1959).
[22]N. El Khayati, R. Cherkaoui El Moursli, J. Rodriguez-Carvajal, G. Andre, N. Blanchard, F. Bouree, G. Collin, and T. Roisnel, Euro. Phys. J. B **22**, 429 (2001).
[23]V. Yushankhai, M. Wolf, K. H. Müller, R. Hayn, and H. Rosner, Phys. Rev. B **62**, 14229 (2000).
[24]J. F. Nossa, M. F. Islam, C. M. Canali, and M. R. Pederson, Phys. Rev. B **85**, 085427 (2012).
[25]D. Coffey, T. M. Rice, and F. C. Zhang, Phys. Rev. B **44**, 10112 (1991).
[26]H. De Raedt, S. Miyashita, K. Michielsen, and M. Machida, Phys. Rev. B **70**, 064401 (2004).
[27]C. D. Hu, J. Phys.: Condens. Matter **24**, 086001 (2012).
[28]K.-C. Liang, W. Zhang, B. Lorenz, Y. Y. Sun, P. S. Halasyamani, and C. W. Chu, Phys. Rev. B **86**, 094414 (2012).
[29]W. G. Zhang and P. S. Halasyamani, Cryst. Growth Des. **12**, 2127 (2012).
[30]I. A. Sergienko and E. Dagotto, Phys. Rev. B **73**, 094434 2006).
[31]J. Romhányi, K. Totsuka, and K. Penc, Phys. Rev. B **83**, 024413 (2011).